# Chapter 3

# Transport, magnetic and structural properties of Mott insulator $MnV_2O_4$ at the boundary between localized and itinerant electron limit

## 3.1 Introduction

In recent years the Vanadium oxide spinels have attracted much attention because of the orbital degeneracy, and the interplay of spin, orbital and lattice degrees of freedom. This interplay arises not only from conventional spin-orbit coupling but also from the fact that the occupation of the specific orbitals with geometrical anisotropy prefers specific types of magnetic interaction in specific direction (the so-called Kugel-Khomskii type coupling) [1]. In spinel Vanadate the magnetic $V^{3+}$ ions with $t_{2g}$ orbital degeneracy are located at vertices of a network of corner sharing tetrahedral that is magnetically frustrating. Many studies have been done to understand the mechanism of these $AV_2O_4$ Vanadates [2-4], where A is a non-magnetic species such as Mg, Zn, or Cd. Usually Vanadates undergo a contraction along the c-axis, which favors the $d_{xy}$ orbital to be occupied by a $t_{2g}$ electron of every $V^{3+}$ ions. The second $t_{2g}$ electron either occupies different $d_{yz}$ and $d_{zx}$ orbitals alternately along the c-axis [5] or occupies the same $d_{yz} \pm id_{zx}$ [6] or forms the more complex pattern [7]. A common feature found in these materials is a sequence of two phase transitions [2-4]. The higher temperature transition is a structural distortion involving a compression of the $VO_6$ octahedra and a consequent parallel lifting of the orbital degeneracy. The orbital ordering is accompanied, at lower temperature by an antiferromagnetic ordering.

Moreover, the $AV_2O_4$ spinels are a family of Mott insulators. Essentially, Mott insulators are paradigmatic examples of strongly correlated materials. The strong-coupling limit, $U >> t$ ($U$ is the inter-atomic Coulomb energy and $t$ is the spin dependent expectation value for the charge transfer between sites), corresponds to materials in which valence electrons are strongly localized in their atomic orbitals (Mott-Hubbard insulator). The opposite weak-coupling limit, $U << t$, corresponds to correlated metals whose electrons are completely delocalized (Paramagnetic metal). This implies that a Mott transition is induced at a critical value $Uc/t$ [8]. These $AV_2O_4$ spinels fulfill the criterion of varying the $t/U$ ratio because of the metal-metal distance can be changed by applying the chemical pressure i.e., by changing the size of the $A^{2+}$ cation [9]. It is highly challenging to characterize the electronic properties of materials when approaching the quantum phase transition (QPT) either from Mott insulator side or from the paramagnetic metal side. The absence of $e_g$ electrons in these vanadates makes direct V-V hybridization between $t_{2g}$

orbitals, the only relevant contribution to the hopping amplitude. Moreover, $t$ is also a function of the interionic distance, $R$. This volume dependency [10] is the basis of the phenomenological Bloch's equation [11] for magnetic insulators: $\alpha_B \approx -3.3$ provided $U$ remains constant. When approached towards itinerant-electron behaviour the $\alpha_B$ value is very sensitive so that it can indicate the applicability of crystal-field theory [12,13]. Blanco-canosa *et al.* have shown that as the V-V separation decreases, $\alpha_B$ value increases progressively in the Mott-insulator region [9]. The large value of $\alpha_B$ is due to the anomalous compressibility near magnetic transition at the crossover from a longer to a shorter equilibrium V-V bond [9].

Recent attention has turned to $MnV_2O_4$ [14-17]. This $MnV_2O_4$ lies in the Mott insulator regime and $\alpha_B \approx -9.9$ [9]. Also, in this case $Mn^{2+}$ is in the $3d^5$ high-spin configuration with no orbital degrees of freedom, and can be regarded as a simple S=5/2 spin. On the other hand, the B-site is occupied by the $V^{3+}$ ion, which takes the $3d^2$ high-spin configuration in the triply degenerate $t_{2g}$ orbital, and has orbital degrees of freedom. $MnV_2O_4$ exhibits a collinear ferrimagnetic ordering at $T_C$=57 K, where the magnetic moments of the Mn and the V sites align in opposite direction. It then exhibits a structural phase transition from a cubic to a tetragonal phase at $T_S$=53 K, with the spin structure becoming non-collinear [14]. It was also observed that the cubic to tetragonal transition could be induced by a magnetic field of few Tesla [15, 16]. In addition, it has been pointed out [18] that the orbital state of $MnV_2O_4$ cannot be explained simply by anti-ferro orbital model. Zn doping also revealed that the structural phase transition from a cubic to a tetragonal phase is a co-operative phenomena dominated by orbital degrees of freedom [15]. Moreover, Zn is non-magnetic and therefore, doping of Zn on Mn site may affect both $T_C$ and $T_S$. In this perspective the detail study of Zn doping in $MnV_2O_4$ will be highly interesting to throw light on the mechanism of $MnV_2O_4$ regarding the appearance of magnetic and structural transitions. On the other hand, Cr doping at the V site may change the orbital ordering as for Cr all the $t_{2g}$ levels are full. In this study, we have investigated the transport, magnetic and structural properties of $MnV_2O_4$ by doping Zn on the Mn site and Cr on the V site. It has been observed that with Zn doping both the Curie temperature ($T_C$) and structural transition temperature ($T_S$) decrease while the gap between them

increases rapidly. On the other hand, with Cr-doping on the V site the $T_C$ remains almost constant but $T_S$ decreases rapidly.

## 3.2 Experimental

Block diagram of the solid state reaction technique, to synthesize Zn and Cr doped $MnV_2O_4$, has been given below.
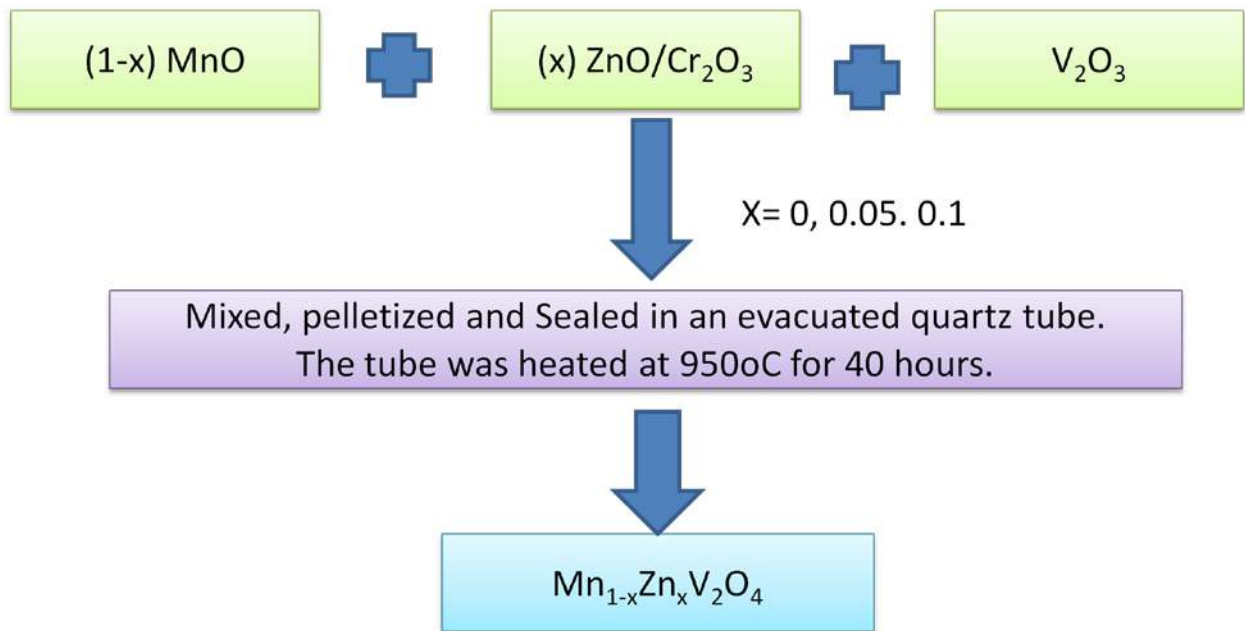


**Fig. 3.1.** *Block diagram of solid state reaction technique to synthesize $Mn_{1-x}Zn_xV_2O_4$ and $Mn(V_{1-x}Cr_x)_2O_4$.*

    The polycrystalline $Mn_{1-x}Zn_xV_2O_4$ and $Mn(V_{1-x}Cr_x)_2O_4$ samples used in this study were prepared by solid state reaction method. Appropriate stoichiometric ratio of MnO, $ZnO/Cr_2O_3$ and $V_2O_3$ were ground thoroughly and pressed into pellets. The pellets were sealed in evacuated quartz tube and heated at 950 $^o$C for 40 hours. The X-ray powder diffraction has been taken using Rigaku MiniFlex II DEXTOP X-ray diffractometer with Cu-Kα radiation. Magnetic measurement was done using MPMS SQUID (Quantum Design) magnetometer with the bulk samples. Data were collected upon warming up the sample. The resistivity and thermoelectric power measurements were performed in a

homemade liquid Nitrogen Cryostat. The thermoelectric power has been measured by differential technique keeping the temperature difference between the two ends of the sample (length ~5 mm) about 0.5 K–1.0 K. The Neutron diffraction measurement was performed on the neutron powder diffractometer (PD2) at Bhabha Atomic Research Centre, Mumbai, India using neutrons of wavelength, $\lambda=1.2443$ Å.

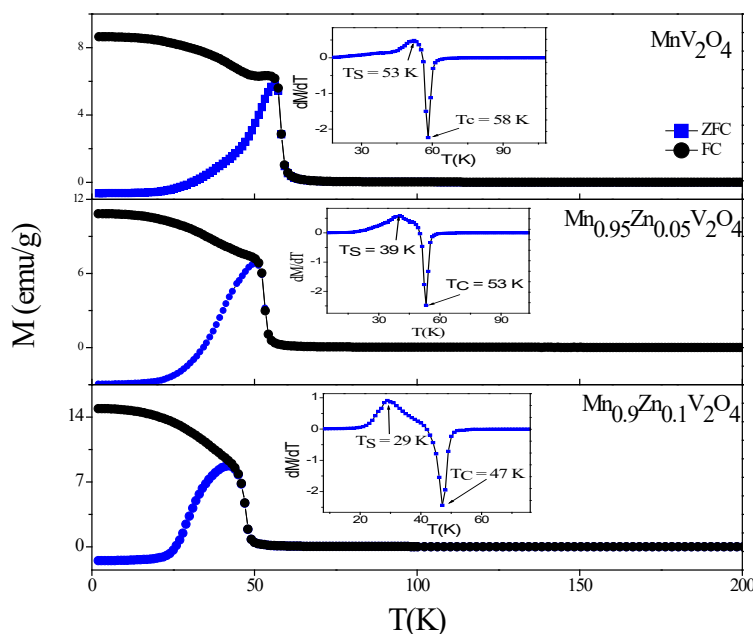## 3.3 Results and Discussion

### 3.3.1 Magnetic Property



**Fig 3.2.** *Temperature variation of magnetization of $Mn_{1-x}Zn_xV_2O_4$ (with x=0, 0.05, 0.1) measured at H=100 Oe. Inset shows the plot of dM/dT vs. T indicating two transitions.*

Fig. 3.2 shows the temperature dependence of magnetization of $Mn_{1-x}Zn_xV_2O_4$ under zero field cooled (ZFC) and field cooled (FC) condition at 100 Oe. The M-T curve of $MnV_2O_4$ exhibits a sharp paramagnetic-ferrimagnetic (PM-FM) phase transition. The Curie temperature $T_C$, defined by the minimum in dM/dT as a function of T, has been determined to be~58K. With further decrease of temperature the ZFC and FC curves exhibit a considerable divergence indicating the presence of magnetic frustration which might be due

to the existence of a long range ordered state [19]. It has been reported that the paramagnetic to ferrimagnetic transition is a second order transition and the transition at the lower temperature (~52K), which is associated with the orbital ordering of V ions (also the structural transition from cubic to tetragonal phase) is first order in nature [14]. Both the $T_C$ and $T_S$ (structural transition temperature) have been determined from the dM/dT vs. T curve (shown in the inset of Fig. 3.2).
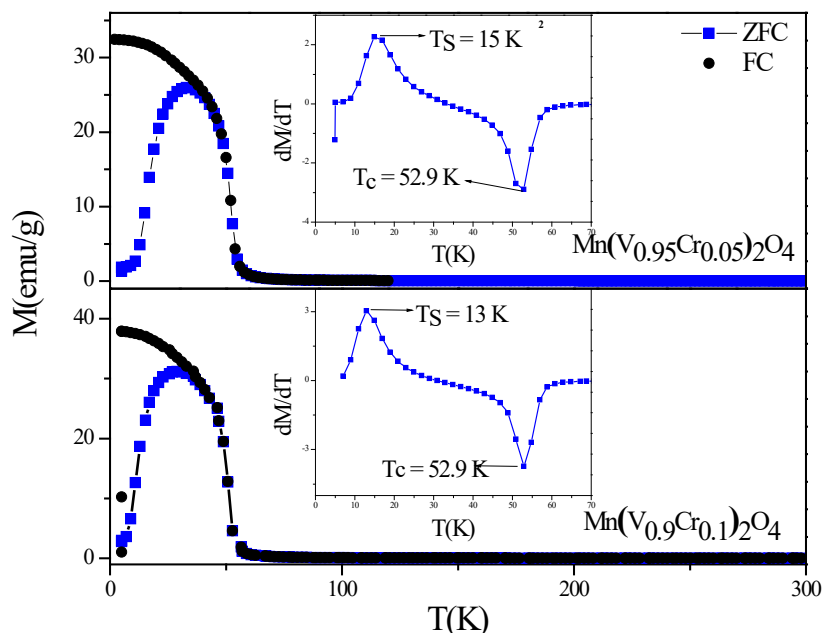


**Fig 3.3.** *Temperature variation of magnetization of Mn(V$_{1-x}$Cr$_x$)$_2$O$_4$ (with x = 0.05, 0.1) measured at H=500 Oe. Inset shows the plot of dM/dT vs. T indicating two transitions.*

For Zn=0.05 and 0.1 the $T_C$ decreased from 58 K (x=0) to 52.5 K and 47 K respectively whereas the $T_S$ decreased from 53 K (for x=0) to 39 K and 29 K respectively. It is to be noted here that the value of the magnetization increases with the Zn content which is also consistent with the report by Adachi *et. al.* [15] which is due to the change of canting angle with Zn doping [15]. Although both $T_C$ and $T_S$ decrease with Zn content, the difference between these two increases with increase of Zn concentration. It has been shown by Garlea *et. al.* [20] that the structural transition is associated with a non-collinear ferrimagnetic structure (Mn spins are non-collinearly oriented with the V spins). As Zn is non-magnetic, with increase of Zn the non-collinear orientation will decrease.

Moreover, homopolar bonding is formed when the metal-metal separation R$\geq$Rc. In homopolar bonding the V-V pairing in the tetragonal phase neither suppresses totally the

spin on a Vanadium ions nor removes geometric frustration completely which leads to a short range magnetic order below $T_C$ (and $T_S$) and an incommensurate spin density wave [9]. This has been confirmed by NMR, muon spin resonance, neutron diffraction and neutron scattering studies [21-23]. In the observed magnetization behaviour the decrease in $T_C$ can be explained as the residual spins on the V-V pairs are reduced with chemical pressure which leads to the decrease of long range magnetic ordering $T_C$. On the other hand, when Cr is doped on the Vanadium site it is observed that with 5% Cr doping the $T_C$ decreases only slightly (Fig. 3.3) and with further increase of Cr (10%) there is no observable change in $T_C$. Initially, with Cr doping due to lattice distortion some change in the spin canting occurs which in effect decreases $T_C$ slightly. With further increase of Cr the structure becomes stable and as a matter of fact no further change in canting takes place which leads to constant value of $T_C$ with Cr content.

## 3.3.2 Structural Analysis

In order to monitor the changes in the crystal and magnetic structure across the transitions we have performed Neutron diffraction and X-ray diffraction experiments. Fig. 3.4 shows the evolution with temperature of integrated intensities of $(220)_T$ reflection obtained from X-ray diffraction. It is observed from the integrated intensity vs. temperature curve that all the three samples undergo a cubic to tetragonal structural transition. For x=0, 0.05 and 0.1 the $T_S$ are, respectively, 50 K, 40 K and 32 K. These values are consistent with those obtained from magnetic measurement. The transition can also be shown from the indexing of peaks at different temperatures. We have shown the splitting of peaks with temperature for x=0, 0.05 and 0.1 samples in Fig. 3.5(a) which clearly shows the occurrence of tetragonal distortion by the splitting of the (400) peak into $(220)_T$ and $(004)_T$ peaks. In Fig. 3.5(b) the systematic occurrence of tetragonal distortion of $MnV_2O_4$ has been shown.
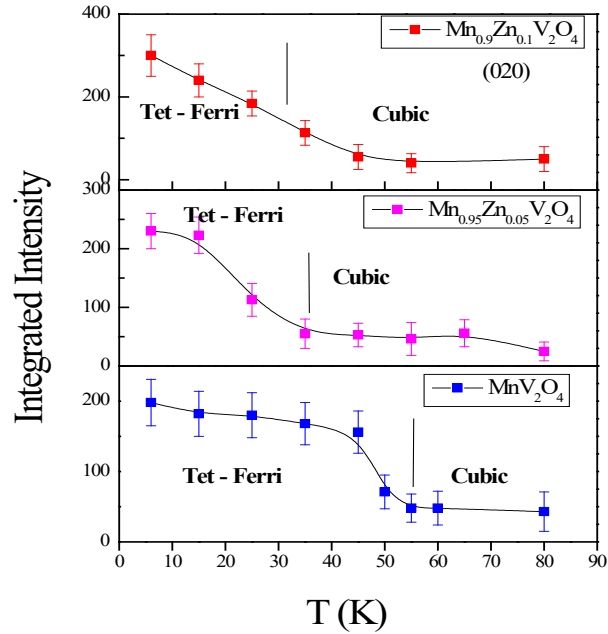
**Fig. 3.4**. *Integrated intensity of (220) for Mn$_{1-x}$Zn$_x$V$_2$O$_4$ (with x=0, 0.05, 0.1).*
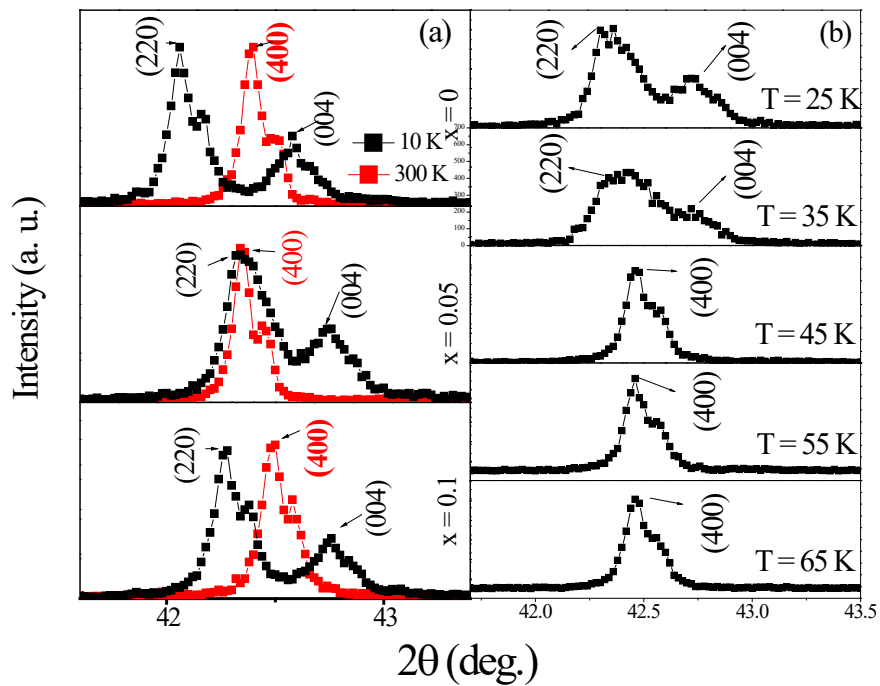


**Fig. 3.5.** *(a) Splitting of 400 → (220)$_T$ + (004)$_T$ of Mn$_{1-x}$Zn$_x$V$_2$O$_4$ (with x=0, 0.05, 0.1) obtained from XRD and (b) shows systematic evolution of Tetragonal distortion for x=0.1 sample.*
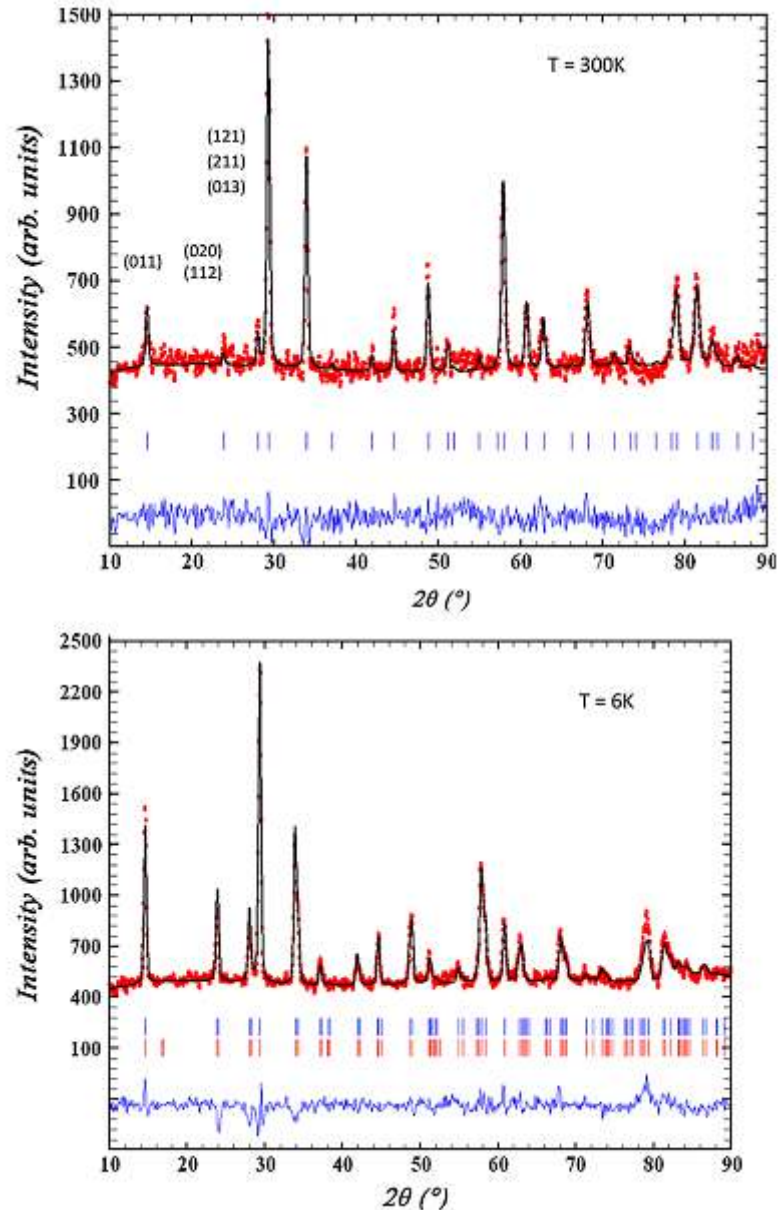
**Fig. 3.6.** *Neutron diffraction pattern of $MnV_2O_4$ at 300 K and 6 K. The tick marks indicate the position of the nuclear (top) and magnetic (bottom) reflections, respectively.*

Fig. 3.6 shows a representative neutron diffraction pattern of $MnV_2O_4$ at 300 K and 6 K. Significant enhancement in the intensity of the first three reflections (indexed in the figure) is observed on lowering of temperature indicating the magnetic contributions to the intensity. We have analyzed the diffraction pattern of all the samples using the Rietveld refinement method above and below the structural transition. The magnetic structure model chosen is similar to that reported by Garlea *et. al.* [20]. The space group used above the $T_S$

is Fd-3m and I4₁/a below the transition. The parameters obtained from combined refinement of X-ray diffraction and neutron diffraction data are summarized in Table 3.1 for $Mn_{1-x}Zn_xV_2O_4$ (where x=0, 0.05 and 0.1) and refinement of X-ray diffraction data of $Mn(V_{1-x}Cr_x)_2O_4$ ( where x =0.05, 0.1) are summarized in Table 3.2. The c/a ratio in the low temperature phase for $MnV_2O_4$ obtained from the fitting is 0.9894, whereas for x=0.05 and 0.1 the values are respectively, 0.9909 and 0.9926. For all the cases the V-O values indicate the $VO_6$ octahedral is compressed along the c-direction and with Zn concentration the distortion decreases.

**Table 3.1.** *Structural parameters (lattice parameters, bond lengths) of $Mn_{1-x}Zn_xV_2O_4$ (with x=0, 0.05, 0.1) samples obtained from neutron and X-Ray Diffraction data refinement. The structural data have been refined with Space group I41/a at 6K and Fd-3 m at 300 K:*

| | 6K | | | | 300K | | |
|---|---|---|---|---|---|---|---|
| Bonds (Å) | X=0.0 | X=0.05 | X=0.1 | Bonds (Å) | X=0.0 | X=0.05 | X=0.1 |
| Mn- O | | 2×2.032(2) | 2.021(2) | Mn- O | 4× 2.043(1) | 4×2.0338(6) | 4×2.0326(9) |
| Mn- O | 4×2.034(3) | 2×2.032(2) | 2.021(2) | | | | |
| V- O | | 2×2.014(3) | 2.022(3) | V - O | 6× 2.023(1) | 6× 2.0249(6) | 6× 2.0234(9) |
| V - O | 2×2.030(3) | | | | | | |
| | 4×2.033(2) | 4×2.027(1) | 2.024(1) | V- V | 3.0130 (1) | 6×3.0105 (1) | 6×3.0105 (1) |
| V- V | | 4×3.0029(2) | 2.9990(2) | | | | |
| V- V | 4×3.0117(2) | 2×3.0167(2) | 3.0102(2) | | | | |
| a (Å) | 6.0555(3) | 6.0333(3) | 6.0203(4) | 8.5220(7) | | 8.5150(3) | 8.5092(9) |
| b (Å) | 6.0555(3) | 6.0333(3) | 6.0203(4) | 8.5220(7) | | 8.5150(3) | 8.5092(9) |
| c (Å) | 8.4726(9) | 8.4546(8) | 8.4507(9) | 8.5220(7) | | 8.5150(3) | 8.5092(9) |
| $M_{Mn}$ $M_V$ | X=0.0 at 6 K 4.7 μB parallel to c. 0.5 μB at an angle with c. | | X=0.05 at 6 K 4.7 μB parallel to c. 0.5 μB at an angle with c. | | X=0.1 at 6 K 4.7 μB parallel to c. 0.5 μB at an angle with c. | | |
| c/a | 0.9894 | 0.9909 | 0.9926 | | | | |

This distortion splits the triply degenerate $t_{2g}$ orbitals into an *xy* orbital with lower energy and doubly degenerate *yz* and *zx* orbital with a higher energy. It has been explained that in $MnV_2O_4$ Orbital ordering occurs immediately after the spin ordering because the

long-range spin ordering endows the orbital system with a one-dimensional character along the c-axis which produces a strong Jahn-Teller lattice distortion coupled with Orbital ordering [24]. In the present investigation also with doping of Zn the Jahn-Teller distortion decreases. Therefore, the more rapid decrease of $T_S$ is due to the fact that with Zn-doping the Jahn-Teller effect decreases which leads to the decrease of the effective exchange interaction between Mn and V which in effect decreases the temperature where non-collinear ferromagnetic state appears resulting the rapid decrease of $T_S$ with Zn doping.

**Table 3.2.** *Structural parameters (lattice parameters, bond lengths) of $Mn(V_{1-x}Cr_x)_2O_4$ (with x=0.05, 0.1) samples obtained from Rietveld refinement of X-ray diffraction data. The structural data have been refined with Space group I41/a at 10K and Fd-3 m at 300K:*

| | | | | | | c/a |
|---|---|---|---|---|---|---|
| $Mn(V_{0.95}Cr_{0.05})_2O_4$ | 10K | a(Å) | 6.034(3) | d(Mn-O)(Å) | 4×2.007(0) | 0.9908 |
| | | b(Å) | 6.034(3) | d(V-O) (Å) | 2×2.031(3), 4×2.038(3) | |
| | | c(Å) | 8.453(9) | d(V-V)(Å) | 2×2.031(3), 4×2.038(3) | |
| | 300K | | | d(Mn-O)(Å) | 4×2.049(8) | |
| | | a(Å) | 8.508(1) | d(V-O) (Å) | 6×2.014(2) | |
| | | | | d(V-V)(Å) | 6×3.008(1) | |
| $Mn(V_{0.9}Cr_{0.1})_2O_4$ | 10K | a(Å) | 6.029(2) | d(Mn-O)(Å) | 4×2.006(6) | 0.9927 |
| | | b(Å) | 6.029(2) | d(V-O) (Å) | 2×2.033(4), 4×2.036(6) | |
| | | c(Å) | 8.462(8) | d(V-V)(Å) | 2×3.014(6), 4×3.003(4) | |
| | 300 K | a(Å) | 8.507(8) | d(Mn-O)(Å) | 4×1.992(3) | |
| | | | | d(V-O) (Å) | 6×2.043(9) | |
| | | | | d(V-V)(Å) | 6×3.008(0) | |

Moreover, for the Cr doped sample the $T_S$ becomes very low. This might be the fact that $Cr^{3+}$ has no orbital ordering (as all $t_{2g}$ levels are full) and as a consequence the orbital ordering decreases with Cr doping resulting lower $T_S$.
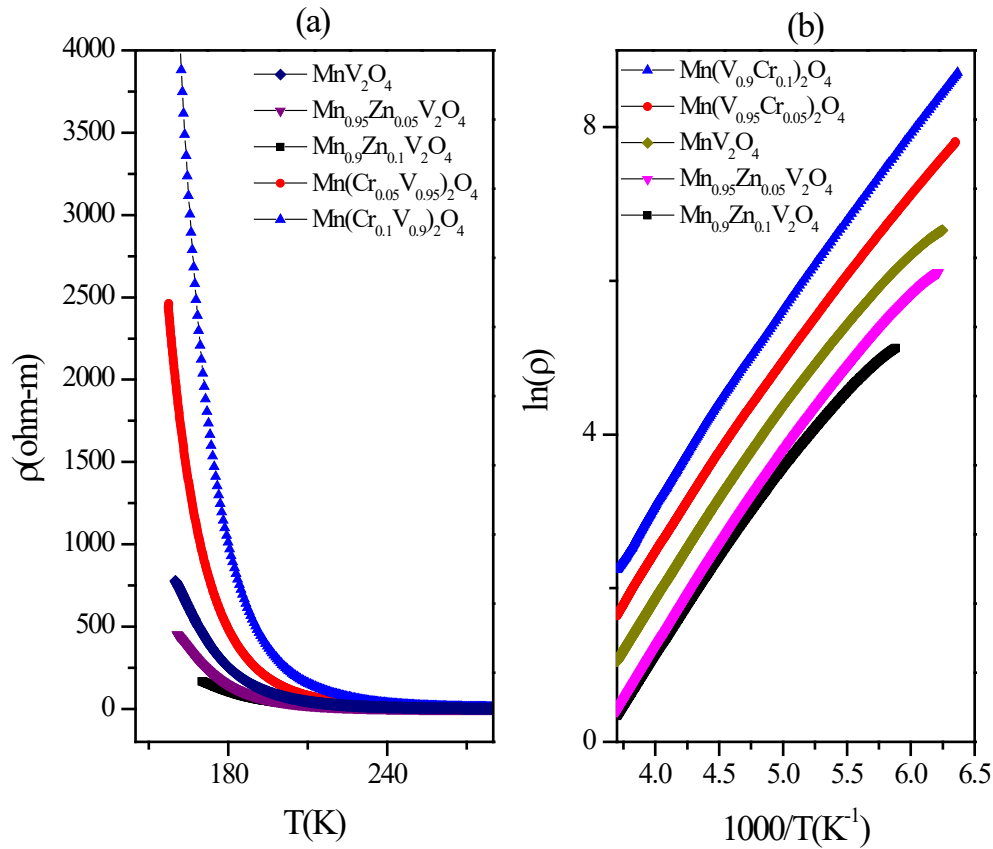
### 3.3.3 Transport Property



**Fig. 3.7.** *Temperature dependent (a) Electrical resistivity of $Mn_{1-x}Zn_xV_2O_4$ (with x=0, 0.05, 0.1) and $Mn(V_{1-x}Cr_x)_2O_4$ (with x = 0.05, 0.1) (b) ln(ρ) vs 1000/T for $Mn_{1-x}Zn_xV_2O_4$ (with x=0, 0.05, 0.1) and $Mn(V_{1-x}Cr_x)_2O_4$ (with x = 0.05, 0.1).*

The temperature dependence of resistivity for Zn and Cr doped $MnV_2O_4$ is shown in Fig. 3.7(a). The resistivity shows semiconducting behaviour within our temperature range of measurement. The resistivity of doped and undoped $MnV_2O_4$ can be well fitted by $\rho=\rho_0 exp(E_a/kT)$ for nearest-neighbour hopping of polarons [Fig. 3.7(b)], where $E_a$ is the

activation energy. With increasing Zn content, the resistivity and $E_a$ both decrease. It has also been mentioned that with increase of Zn content $T_C$ also decreases. Studies on $AV_2O_4$ have indicated that with decreasing V-V distance, these Vanadates approach from localization limit to the itinerant-electron limit. $MnV_2O_4$ is well inside the localization limit [25] and this shows abnormal properties. For example, $MnV_2O_4$ shows a large pressure dependence of $T_C$ which leads to phenomenological Bloch's parameter $\alpha_B$=-9.9 [25], showing the breakdown of the Bloch law [26].
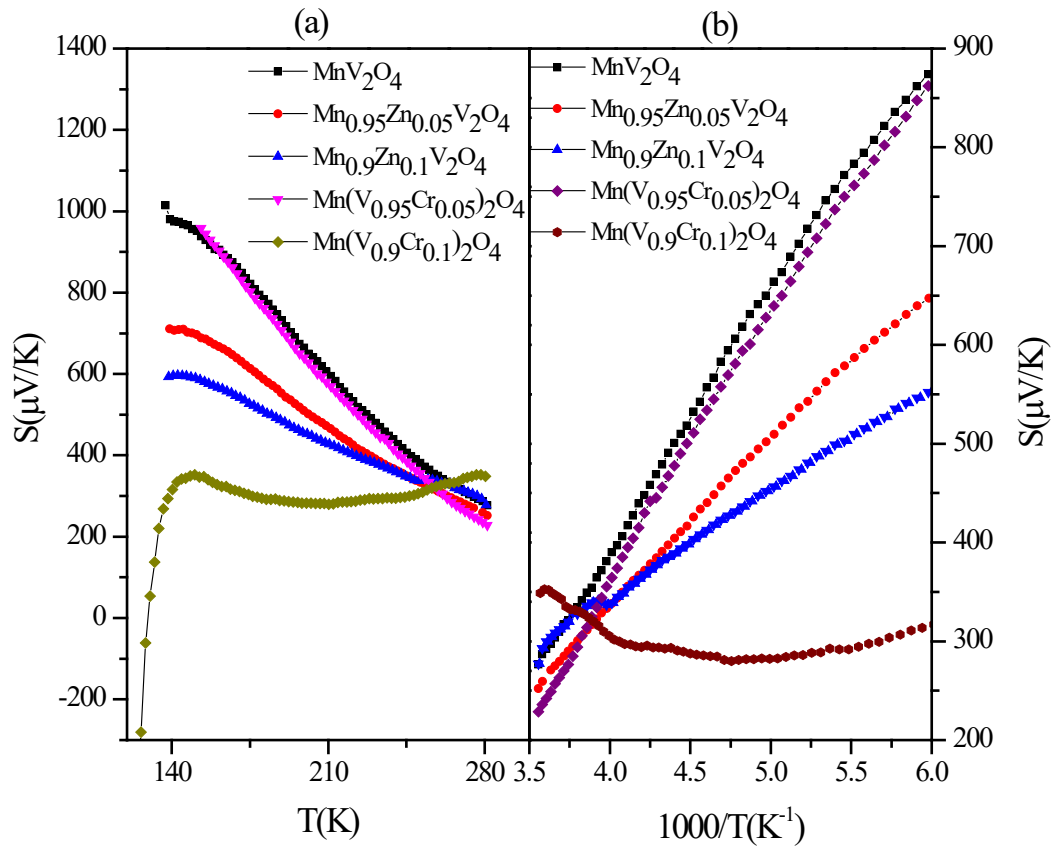


**Fig. 3.8.** *Seebeck coefficient as a function of (a) Temperature and (b) 1000/T for $Mn_{1-x}Zn_xV_2O_4$ (with x=0, 0.05, 0.1) and $Mn(V_{1-x}Cr_x)_2O_4$ (with x = 0.05, 0.1).*

In the present investigation as we increase the Zn content (i.e. the chemical pressure) it is also observed the estimated Bloch's parameter is very large. The large $\alpha_B$ is due to an anomalous compressibility near $T_C$ as predicted for a double-well potential at the crossover from a longer to a shorter equilibrium V-V bond can perturb the periodic potential to trap the charge carriers, which gives a dominant variable range hopping (VRH), given by

$\rho=\rho_0\exp[To/T^{1/4}]$, transport behaviour [27]. For VRH model, the constant $T_0=\alpha^3/k_BN(E_F)$, where $\alpha^{-1}$ is the localization length, $k_B$ is the Boltzmann constant, and $N(E_F)$ is the density of localized states at Fermi level. It is not possible that the Zn doping on the Mn site can change the $N(E_F)$ which in effect can account for the large decrease of $T_0$. But, the decrease of $T_0$ may indicate the increase of localization length $\alpha^{-1}$ which leads to electronic delocalization.

**Table 3.3.** *Transport parameters $E_a$ (obtained from resistivity data using small polaron hopping model), $E_s$ (obtained from thermo-electric power data) and $T_o$ (obtained from resistivity data using Variable range hopping model) for the spinels $Mn_{1-x}Zn_xV_2O_4$ (with x=0, 0.05, 0.1) and $Mn(V_{1-x}Cr_x)_2O_4$ (with x = 0.05, 0.1):*

| | $E_a$ (eV) (Arrhenius Model) | $E_s$ (eV) | $T_o$(K) (VRH model) |
|---|---|---|---|
| $MnV_2O_4$ | 0.224358 | 0.2666 | $5.12\times10^8$ |
| $Mn_{0.95}Zn_{0.05}V_2O_4$ | 0.210328 | 0.1709 | $4.15\times10^8$ |
| $Mn_{0.9}Zn_{0.1}V_2O_4$ | 0.197398 | 0.1078 | $3.52\times10^8$ |
| $Mn(V_{0.95}Cr_{0.05})_2O_4$ | 0.225844 | 0.2805 | $9.08\times10^8$ |
| $Mn(V_{0.9}Cr_{0.1})_2O_4$ | 0.234464 | 0.0401 | $12.27\times10^8$ |

On the other hand, with increasing Cr content both resistivity and $E_a$ increase. Moreover $T_0$ decreases with increase of Cr content which in effect increase the localization. The thermoelectric power (TEP) data for Zn doped and Cr doped $MnV_2O_4$ samples are shown in Fig. 3.8(a). It is observed that with Zn doping the TEP value decreases which clearly indicates that with decrease of V-V separation the system moves towards the itinerant electron limit. But interestingly it is observed that with Cr doping although the metal-metal separation increases the TEP value decreases and with 10% doping below a

critical temperature it drops abruptly. The activation energy has been estimated from the resistivity data using the small polaron hopping model. According to the small polaron theory the thermo-power can be expressed as

$$S(T)=k_B/e[E_s/k_BT + \alpha] \tag{3.1}$$

where, $E_s$ is the activation energy for the TEP and $\alpha$ is the sample dependent constant. All the samples (except the 10% Cr doped sample) obey the prediction of the small polaron theory, as S vs 1000/T curves fit well with straight lines (Fig. 3.8(b)). From the linear fit of the curves the obtained activation energies for thermo-power along with those obtained from resistivity data are shown in Table-3.3. The different values of the activation energies for the resistivity and the TEP are consistent with the conduction due to hopping of charge carriers. Moreover, the S(T) value is large and positive which indicates that there is only a low density of mobile holes in these vanadates and the thermally activated behaviour of small polarons for all these vanadates is observed. Therefore, the possibility of the existence of the large polaron which forms due to non-stoichiometry can be excluded. At high temperature the estimated activation energy, $E_s$ is found to decrease with increase of Zn content but to increase initially with increase of Cr (5%) content. But when 10% Cr is doped the Es value decreases abruptly. The $E_s$ is directly proportional to the trapping enthalpy. Therefore, with increase of Zn content a trapping out of mobile holes decreases whereas for low Cr doping the trapping increases. This indicates that when Zn is doped the system moves from localized to itinerant electronic behavior whereas for Cr doping the system moves from itinerant to localized electronic behavior which is the characteristic of a narrow band where as mentioned above the appearance of a double-well bond potential introduces lattice instabilities. For 10% Cr doping the TEP value (also $E_s$) decreases and below 140 K sign change (positive to negative) occurs. It may happen that with 10% Cr doping band gap increases which may lead to the decrement of the mobility of the polaronic holes than the mobility of the electronic polarons at low temperature. Therefore for the region of the localized electron limit the mobility of the electronic polarons dominate and at the crossover from itinerant to localized electronic behavior the mobility of the polaronic holes dominate.

## 3.4 Conclusion

The size of the magnetization increases with the Zn content which is due to the change of canting angle with Zn doping. With increase of Zn the non-linear orientation of Mn spins with the V spins decreases. The decrease in $T_C$ with Zn doping can be explained as the residual spins on the V-V pairs are reduced with chemical pressure which leads to the decrease of long range magnetic ordering. The rapid decrease of $T_S$ is due to the decrease of Jahn-Teller effect which leads to the decrease of the effective exchange interaction between Mn and V resulting the decrease of $T_S$ rapidly. It is observed from the VRH model that the Zn doping on the Mn site cause the increase of localization length $\alpha^{-1}$ which leads to electronic delocalization. But, with increasing Cr content the localization increases. Therefore, when Zn is doped the system moves from localized to itinerant electronic behavior whereas for Cr doping the system moves from itinerant to localized electronic behavior which is the characteristic of a narrow band where the appearance of a double-well bond potential introduces lattice instabilities. For 10% Cr doping the TEP value decreases and below 140K sign change (positive to negative) occurs. With the 10% Cr doping band gap increases which may lead to the decrement of the mobility of the polaronic holes than the mobility of the electronic polarons at low temperature. Therefore for the region of the localized electron limit the mobility of the electronic polarons dominate and at the crossover from itinerant to localized electronic behavior the mobility of the polaronic holes dominate.

# References

[1]. Kugel, K. I. and Khomskii, D. I., Crystal Structure and Magnetic properties of substances with orbital degeneracy., J. Exp. Theo. Phys., 37, 725-730, 1973.

[2]. Mamiya, H., Onoda, M., Furubayashi, T., Tang, J. and Nakatani, I., Structural and magnetic studies on vanadium spinel $MgV_2O_4$, J. Appl. Phys., 81, 5289-5291, 1997.

[3]. Ueda, Y. and Fujiwara, N., Magnetic and Structural Transitions in $(Li_xZn_{1-x})V_2O_4$ with the Spinel Structure, J. Phy. Soc. Jpn., 66, 778-783, 1997.

[4]. Nishiguchi, N. and Onoda, M., A pseudotetramer in the geometrically frustrated spinel system $CdV_2O_4$, J. Phys. Condens. Matter, 14, L551-L557, 2002.

[5]. Tsunetsugu, H. and Motome, Y., Magnetic transition and orbital degrees of freedom in vanadium spinels, Phys. Rev. B, 68, 060405/1-060405/4, 2003.

[6]. Tchernyshyov, O., Structural, Orbital and Magnetic Order in Vanadium Spinels, Phys. Rev. Lett., 93, 157206/1-157206/4, 2004.

[7]. Khomskii, D. I. and Mizokawa, T., Orbitally Induced Peierls State in Spinels, Phys. Rev. Lett., 94, 156402/1-156402/4, 2005.

[8]. Brinkman, W. F. and Rice, T. M., Application of Gutzwiller's Variational Method to the Metal-Insulator Transition, Phys. Rev. B, 2, 4302-4304, 1970.

[9]. Blanco-Canosa, S., Rivadulla, F., Pardo, V., Baldomir, D., Zhou, J. S., García-Hernández, M., López-Quintela, M. A., Rivas, J. and Goodenough, J. B., Enhanced Pressure Dependence of Magnetic Exchange in $AV_2O_4$ Spinels Approaching the Itinerant Electron Limit, Phys. Rev. Lett., 99,1872 01, 2007.

[10]. Harrison, W. A., Electronic structure and the properties of solid: The Physics of the chemical bond (W. H. Freeman & co. San Francisco, 1980), 1980.

[11]. Bloch, D., The 103 law for the volume dependence of superexchange, J. Phys. Chem. Solids, 27, 881-885, 1966.

[12]. Zhou, J. S. and Goodenough, J. B., Pressure-Induced Transition from Localized Electron Toward Band Antiferromagnetismin $LaMnO_3$, Phys. Rev. Lett., 89, 087201/1-087201/4, 2002.

[13]. Goodenough, J. B., Longo, J. M. and Kafalas, J. A., Band antiferromagnetism and the new perovskite $CaCrO_3$, Mater. Res. Bull., 3, 471-481, 1968.

[14]. Plumier, R. and Sougi, M., Observation of a first order transition in the ferrimagnetic spinel $MnV_2O_4$, Solid State Commun., 64, 53-55, 1987.

[15]. Adachi, K., Suzuki, T., Kato, K., Osaka, V., Takata, M. and Katsufuji, T., Magnetic-Field Switching of Crystal Structure in an Orbital-Spin-Coupled System:$MnV_2O_4$, Phys. Rev. Lett., 95, 197202/1-197202/4, 2005.

[16]. Suzuki, T., Katsumura, M., Taniguchi, K., Arima, T. and Katsufuji, T., Orbital Ordering and Magnetic Field Effect in $MnV_2O_4$, Phys. Rev. Lett., 98, 127203/1-127203/4, 2007.

[17]. Baek, S. H., Choi, K. Y., Reyes, A. P., Kuhns, P. L., Curro, N. J., Ramanchandran, V., Dalal, N. S., Zhou, H. D. and Wiebe, C. R., Ac susceptibility and $^{51}V$ NMR study of $MnV_2O_4$, J. Phys. Condens. Matter, 20, 135218/1-135218/6, 2008.

[18]. Chung, J. H., Kim, J. H., Lee, S. H., Sato, T. J., Suzuki, T., Katsumura, M. and Katsufuji, T., Magnetic excitations and orbital physics in the ferrimagnetic spinels $MnB_2O_4$ (B=Mn,V), Phys. Rev. B, 77, 054412/1-054412/5, 2008.

[19]. Huang, Y.,Qu, Z. and Zhang, Y., The magnesium doping effect of the vanadate spinel $MnV_2O_4$, J. Mag. Mag. Materials, 323, 975-979, 2011.

[20]. Garlea, V. O., Jin, R., Mandrus, D., Roessli, B., Huang, Q., Miller, M., Schultz, A. J. and Nagler, S. E., Magnetic and Orbital Ordering in the Spinel $MnV_2O_4$, Phys. Rev. Lett., 100, 066404/1-066404/4, 2008.

[21]. Uttgen, N. B., Krimmel, A., Loidl, A., Klemm, M., Horn, S., Noakes, D. R., Schreier, E. and Kalvius, G. M., Magnetic correlations in frustrated $LiV_2O_4$ and $ZnV_2O_4$, Physica B, 703, 312–313, 2002.

[22]. Rechuis, M., Krimmel, A., Buttgen, N., Loidl, A. and Prokofiev, A., Crystallographic and magnetic structure of $ZnV_2O_4$, Eur. Phys. J. B, 35, 311-316, 2003.

[23]. Lee, S. H., Louca, D., Ueda, H., Park, S., Sato, T. J., Isobe, M., Ueda, Y., Rosenkranz, S., Zschack, P., Íñiguez, J., Qiu, Y. and Osborn, R., Orbital and Spin Chains in $ZnV_2O_4$, Phys. Rev. Lett., 93, 156407/1-156407/1, 2004.

[24]. Zhou, H. D., Lu, J. and Wiebe, C. R., Spin ordering and orbital ordering transitions in $MnV_2O_4$, Phys. Rev. B 76, 174403/1-174403/6, 2007.

[25]. Goodenough, J. B., Structure & Bonding (Springer-Verlag, Berlin, 2001), 98, Chaps. 1 and 2, 2001.

[26]. Pardo, V., Blanco-Canosa, S., Rivadulla, F., Khomskii, D. I., Baldomir, D., Wu, H. and Rivas, J., Homopolar Bond Formation in $ZnV_2O_4$ Close to a Metal-Insulator Transition, Phys. Rev. Lett., 101, 256403/1-256403/1/4,2008.

[27]. Kismarahardja, A., Brooks, J. S., Kiswandhi, A., Matsubayashi, K., Yamanaka, R., Uwatoko, Y., Whalen, J., Siegrist, T. and Zhou, H. D., $Co[V_2]O_4$: A Spinel Approaching the Itinerant Electron Limit, Phys. Rev. Lett., 106, 056602/1-056602/4, 2011.